ORIGINAL SCIENTIFIC PAPER OPEN ACCESS

Comparative numerical study of star-shaped auxetic structures with negative Poisson's ratio

Vladimir Sinđelić[1*], Snežana Ćirić-Kostić[1]

[1] University of Kragujevac, Faculty of Mechanical and Civil Engineering, Kraljevo, Serbia

ARTICLE INFO

[*] **Correspondence:** sindjelic.v@mfkv.kg.ac.rs

DOI: 10.5937/engtoday2600004S

UDC: 621(497.11) **ISSN:** 2812-9474

Article history: Received 29 December 2025; Revised 28 January 2026; Accepted 3 February 2026

ABSTRACT

Mechanical metamaterials with a negative Poisson's ratio, commonly referred to as auxetic materials, have attracted increasing attention due to their unconventional deformation mechanisms and enhanced energy absorption capabilities. In this study, a comprehensive numerical investigation of the mechanical properties of four two-dimensional star-shaped auxetic structures is presented. In addition to the conventional 2D arc star-shaped (2D-AS), improved 2D arc star-shaped (*i*2D-AS), and classical star-shaped (2D-SS) structures, a novel tangent 2D arc star-shaped structure (*t*2D-AS) is proposed by modifying the geometry of the original 2D-AS configuration. Finite element simulations were performed using periodic boundary conditions to evaluate the negative Poisson's ratio and Young's modulus under uniaxial loading for different sets of geometric parameters. The numerical model was validated through comparison with available theoretical results for selected structures, demonstrating good agreement. The obtained results indicate that the newly introduced *t*2D-AS structure exhibits the lowest relative density among the analyzed configurations, while maintaining auxetic behavior and competitive stiffness characteristics. Furthermore, the influence of mesh density and the number of unit cells on the calculated Poisson's ratio was investigated using $n \times n$ models, confirming the robustness and consistency of the numerical approach. The findings of this study provide valuable insights into the structure property relationships of star-shaped auxetic metamaterials and establish a solid foundation for future analytical modeling, experimental validation, and energy absorption analyses.

KEYWORDS

Negative Poisson's ratio, Mechanical metamaterial, Auxetic, Geometrical design, Arc star-shaped structure

1. INTRODUCTION

Mechanical metamaterials with a negative Poisson's ratio are artificially designed cellular structures intended to impart unconventional mechanical properties to materials, such as a negative value of the Poisson's ratio [1,2]. In the literature, these materials are commonly referred to as auxetic materials (the term *auxetic* originates from the Greek word meaning "to increase"). Due to the fact that auxetic materials contract laterally under compressive loading, they exhibit excellent energy absorption capabilities during impact events [3]. Consequently, auxetic structures have attracted significant attention across various engineering and industrial applications.

Among different classes of auxetic metamaterials, particular interest has been directed toward structures classified *as* re-entrant types [4]. These structures are typically designed using beams or plates and can be re-entrant in one, two, or multiple directions. Depending on their geometric configuration, re-entrant structures can be further categorized into two-dimensional (2D) and three-dimensional (3D) systems [4].

This study represents an extended and significantly enhanced version of a preliminary conference paper presented in Ref. [5], providing a more detailed numerical investigation of the influence of geometric parameter variations on four types of star-shaped auxetic structures. The geometric characteristics of all analyzed structures are based on the reference structure reported in Ref. [6], while the remaining structures considered for comparison and their mechanical properties can be found in Refs. [6–8]. In addition, the final part of this study numerically examines the influence of the Poisson's ratio on an $n \times n$ model, aiming to assess the effect of the number of unit cells on the overall mechanical response.

2. GEOMETRICAL DESIGN OF THE 2D STAR STRUCTURE

In Fig. 1(a–d), four representative volume elements (RVE in the further) are presented. Starting from the original 2D Arc Star-Shaped structure (2D-AS in the further) [9] shown in Fig. 1(a), three additional structures were designed (Fig. 1(b–d)) while preserving the geometric parameters of the basic 2D-AS RVE. The modification leading to the improved 2D arc star-shaped structure (*i*2D-AS in the further), illustrated in Fig. 1(b), is described in detail in Ref.[6].

The *t*2D-AS RVE shown in Fig. 1(c) was obtained by removing the straight segments and a portion of the arc of the 2D-AS structure, as indicated by the red line. From the intersection point of the straight rods, two additional rods were introduced, marked by the purple lines, which are tangent to the arc of the original 2D-AS structure. Owing to this construction approach, the resulting structure is denoted as tangent 2D-AS (*t*2D-AS).

The classical star structure (2D-SS), shown in Fig. 1(d), was derived in a similar manner in order to preserve the geometric parameters of the 2D-AS RVE. The only difference with respect to the *t*2D-AS structure is that the rods tangent to the arc of the 2D-AS structure were extended until they intersected the vertical and horizontal rods, as indicated by the green lines in Fig. 1(d).

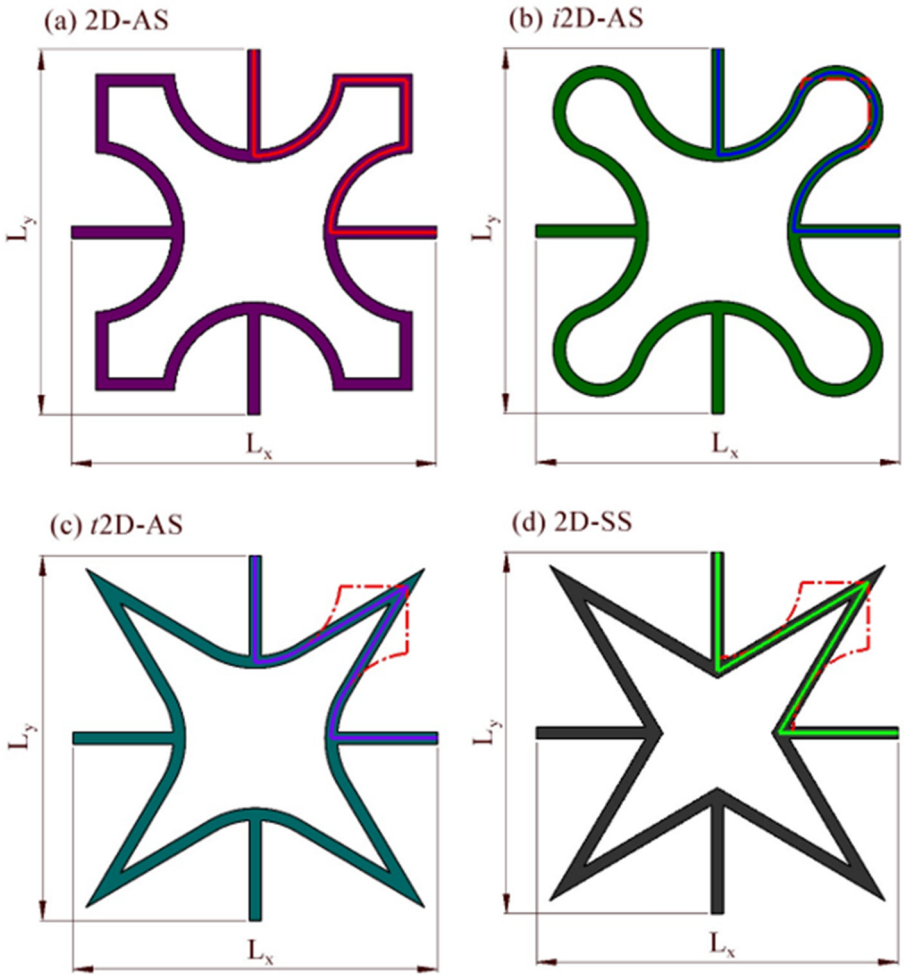

Figure 1: Geometrical parameters of Star-Shaped Structures [5,6,9]: (a) 2D-AS; (b) *i*2D-AS; (c) *t*2D-AS; (c) 2D-SS

2.1. Determination of relative density of four RVE types

All four structures share the same set of geometric parameters defined for the 2D-AS structure. These parameters include the total horizontal and vertical lengths of the structure, denoted as L_x and L_y, respectively (see Fig. 1(a–d)), as well as the half-length L, height h, depth d, thickness t, arc radius r, and arc angle θ, as illustrated in Fig. 2(a–d). The design coefficients a and b are required to satisfy the conditions $0 < a < 1$and $0 < b < 1$[5,6,9].

Based on the relationships between the geometric parameters ah and bh, the arc angle θ and the arc radius r can be determined, as defined in Ref. [6], according to the following expressions:

$$\theta = 2\arctan\frac{bh}{ah} \tag{1}$$

$$r = \frac{ah}{\sin\theta} \tag{2}$$

According to Fig. 2(a), the expression for the relative density of the 2D-AS structure can be derived as follows [9]:

$$\rho_{r2D-AS} = \frac{t\pi\theta(ah)^2}{180l^2\sin^2\theta} + \frac{2t(l+bh-ah)}{l^2} \tag{3}$$

For the geometric description of the *i*2D-AS RVE, in addition to the geometric parameters inherited from the 2D-AS structure, several new parameters are introduced. These include an arc with a new radius R, the arc angle ψ associated with the truncated radius r, the angle φ, which represents the difference between the original angle θ and the new angle ψ corresponding to radius r, as well as the angle α. The dependence of these parameters on ah and bh is described in detail in Ref. [6]. Accordingly, the relative density of the *i*2D-AS structure is given by the following expression [6]:

$$\rho_{ri2D-AS} = \left(L - h + bh + (\pi + 2\alpha)R + 2r\psi\right)\frac{t}{L^2} \tag{4}$$

The geometric description of the *t*2D-AS structure requires the introduction of two additional geometric parameters in order to express it as a function of the geometric parameters of the 2D-AS structure. These parameters are the length of the rod l, which is tangent to a portion of the arc with radius r, and the angle γ, defined as the angle between the rod l and the removed vertical and horizontal rods of the 2D-AS structure, as illustrated in Fig. 2(c) [5].

To determine the rod length l and the angle γ as functions of the geometric parameters ah and bh, the following two equations are employed, respectively [5]:

$$l = \frac{h}{\cos\gamma} - r\tan\gamma \tag{5}$$

$$\frac{(r - h\sin\gamma)}{\cos\gamma} = r\cos\theta \tag{6}$$

The relative density of the *t*2D-AS RVE can then be expressed as [5]:

$$\rho_{rt2D-AS} = \left(2r\gamma + 2\frac{h - r\sin\gamma}{\cos\gamma} + L - h + bh\right)\frac{t}{L^2} \tag{7}$$

The RVE of the 2D-SS structure introduces one additional geometric parameter l_h, which represents the length of the rod that is tangent to the removed arc r of the 2D-AS structure and intersects the horizontal and vertical rods. The angle γ is adopted from the *t*2D-AS structure (see Fig. 2(d)) [5].

To calculate the parameter l_h as a function of the geometric parameters ah and bh, the following expression is used [5]:

$$lh = \frac{h}{\cos\gamma} \tag{8}$$

Accordingly, the relative density of the 2D-SS RVE can be represented as [5]:

$$\rho_{r2D-SS} = \left(2\frac{h}{\cos\gamma} + L - h + h\tan\gamma\right)\frac{t}{L^2} \tag{9}$$

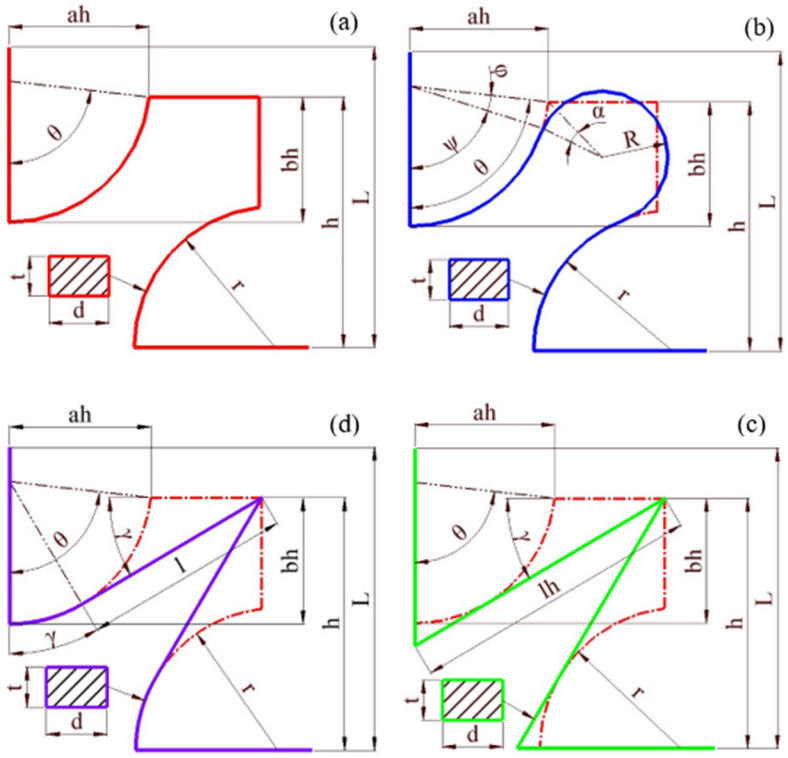

Figure 2: Geometric parameters of the studied structures [5]: (a) 2D-AS; (b) *i*2D-AS; (c) *t*2D-AS; (d) 2D-SS.

2.2. Values of geometric parameters and comparison of relative densities of the structures

For the analysis of the four types of structures, two parameter sets were considered. In the first set, ahvaries from 10 mm to 18 mm in steps of 2 mm, while bh is kept constant. In the second set, bh varies from 10 mm to 16 mm in steps of 2 mm, while ah remains constant [6,9]. All other geometric parameters are identical in both sets and are summarized in Table 1.

Table 1: Geometric parameter values for all star-shaped structures.

Parameters in mm	***Set1***	***Set2***
h	25	25
L	30	30
ah	10, 12, 14, 16, 18	12.5
bh	12.5	10, 12, 14, 16
t	2	2
d	3	3

The relative density values for all four types of structures are presented in Tables 2 and 3 for both parameter sets. A graphical representation of the variation in relative density is shown in Fig. 3.

Table 2: Relative density values of the structures for the variation of the geometric parameter ah.

ah		*10*	*12*	*14*	*16*	*18*
ρ_r	2D-AS	0.1872	0.1827	0.1792	0.1761	0.1736
	i2D-AS	0.1708	0.1735	0.1748	0.1750	0.1742
	t2D-AS	0.1640	0.1642	0.1644	0.1647	0.1650
	2D-SS	0.1696	0.1710	0.1730	0.1757	0.1794

Table 3: Relative density values of the structures for the variation of the geometric parameter bh.

bh		*10*	*12*	*14*	*16*
ρ_r	2D-AS	0.1657	0.1784	0.1919	0.2062
	i2D-AS	0.1650	0.1722	0.1794	0.1868
	t2D-AS	0.1640	0.1642	0.1644	0.1647
	2D-SS	0.1579	0.1686	0.1809	0.1950

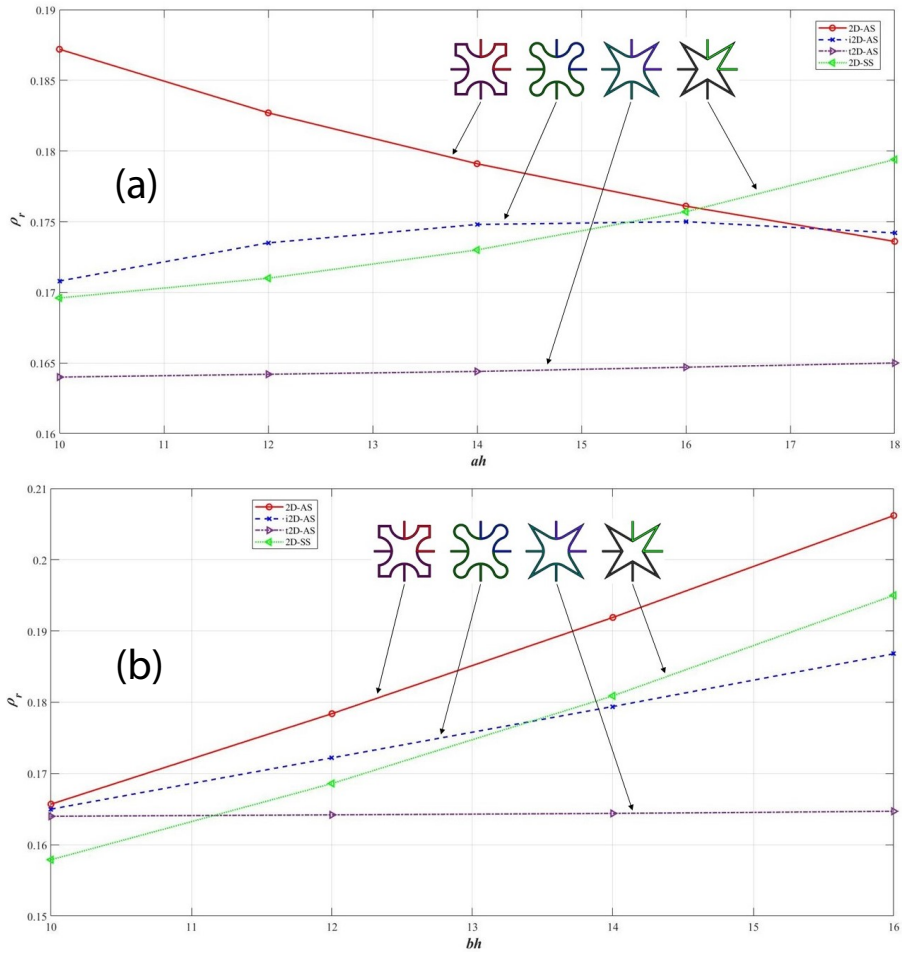

Figure 3: Variation of relative density with geometric parameters: (a) ah [5]; (b) bh.

In both cases, the *t*2D-AS structure exhibits a lower relative density compared to the other three structures. As shown in Tables 2 and 3, for the ahrange between 10 mm and 16 mm, the relative density of *t*2D-AS remains constant, similar to the range in which bh varies between 12 mm and 16 mm.

3. NUMERICAL MODEL

All four types of metamaterials, with varying geometric parameters, were designed in SolidWorks. For the numerical analysis of the influence of Poisson's ratio and Young's modulus on the metamaterials, the ANSYS Workbench Static Structural module was employed. The material considered in the numerical analysis is isotropic, with the following properties: Young's modulus $E_m = 1740$ MPa, Poisson's ratio $\nu_m = 0.4$, and density $\rho_m = 1150$ kg/m³ [5,9].

For all analyzed models, the Hex Dominant meshing method was applied, with the element order set to *Use Global Setting* and the free face mesh type specified as Quad/Tri. This configuration ensures the inclusion of the Solid186 element, which is a higher-order 3D element defined by 20 nodes, each with three degrees of freedom. Solid186 is efficient and well-suited for modeling irregular meshes in CAD-designed models; however, its generation requires the presence of other element types [10,11].

The element size was varied between 0.25 mm and 1.75 mm in increments of 0.25 mm. Two mesh quality criteria, *Skewness* and *Orthogonal Quality*, were employed to determine the optimal element size. The average values of these parameters were calculated and compared with the recommendations listed in Table 4. For this evaluation, all four star-shaped structures were analyzed using a geometric parameter value of $ah = 14$ mm, and the resulting element was subsequently applied in all other models. The average values of *Skewness* and *Orthogonal Quality* for the analyzed structures are presented in Table 5. Based on the data from Tables 4 and 5, all element sizes meet the required criteria [11,12].

For the simulation of a single periodic boundary condition (PBC) [12], an element size of 0.25 mm was used. In subsequent analyses involving $n \times n$cells, a larger element size of 1.5 mm was adopted. Consequently, the Solid186 element becomes the dominant type, comprising approximately 97 % of the elements in all analyzed models. The remaining elements, present in smaller proportions, include Solid187, Conta174, and Targe170. An example of the generated mesh for the *i*2D-AS structure is shown in Fig. 4.

Table 4: Recommended values for mesh quality parameters "*Skewness*" and "*Orthogonal Quality*" [11].

Quality	*Unacceptable*	*Bad*	*Acceptable*	*Good*	*Very good*	*Excellent*
Skewness	0.98-1.00	0.95-0.97	0.80-0.94	0.50-0.80	0.25-0.50	0-0.25
Orthogonal	0-0.001	0.001-0.14	0.15-0.20	0.20-0.69	0.70-0.95	0.95-1.00

Table 5: Average values of "Skewness" and "Orthogonal Quality" for structures with $ah = 14$ mm.

Element size in mm			**1.75**	**1.50**	**1.25**	**1.00**	**0.75**	**0.50**	**0.25**
ah14	2D-AS	Skewness	0.3899	0.3085	0.4331	0.3818	0.1555	0.1929	0.1626
		Orthogonal	0.6654	0.7746	0.6406	0.7024	0.9337	0.8989	0.9106
	*i*2D-AS	Skewness	0.5004	0.2785	0.3160	0.3842	0.2403	0.1757	0.1227
		Orthogonal	0.5307	0.8113	0.7642	0.6950	0.8509	0.9067	0.9330
	*t*2D-AS	Skewness	0.5464	0.3011	0.1671	0.2759	0.1801	0.1898	0.0094
		Orthogonal	0.4856	0.7767	0.8998	0.8060	0.8935	0.8842	0.9574
	2D-SS	Skewness	0.5673	0.3578	0.1384	0.3545	0.2312	0.1604	0.1111
		Orthogonal	0.4682	0.7092	0.9145	0.7073	0.8473	0.9050	0.9416

To simulate periodic boundary conditions (PBC, hereafter) on the AS structure, boundary conditions were applied at the ends of the metamaterial, as commonly adopted in previous studies [12–16] and illustrated in Fig. 5. Remote displacements were applied at the ends of rods A, B, and C, while end D was left free. Specifically, at end A of the rod, only horizontal displacement along the x-axis was allowed; at end B, vertical displacement along the y-axis was free. At end C, a fixed vertical displacement of -3 mm was applied, while horizontal displacement remained unconstrained. All boundary conditions at the rod ends are summarized in Table 6.

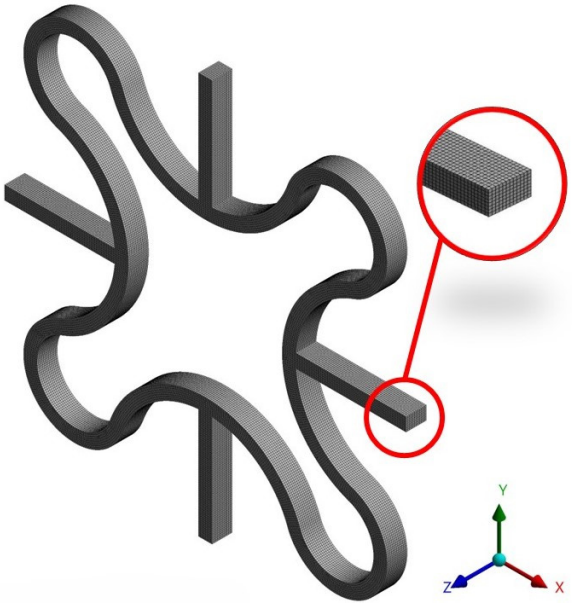

Figure 4: Generated mesh for the i2D-AS structure.

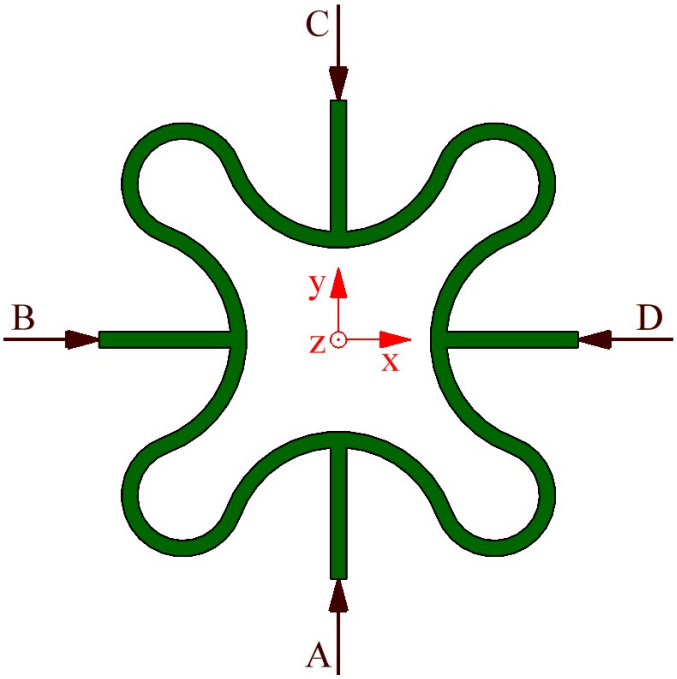

Figure 5: Example of periodic boundary conditions (PBC) applied to the *i*2D-AS structure [5].

The software output includes the reaction force in the vertical direction at point C, which is used to calculate the Young's modulus, and the horizontal displacement at point D, which is required for determining the Poisson's ratio of the metamaterial.

Table 6: Boundary conditions applied to the finite element models.

Boundary conditions	***Case for the FE model***
A	*f_x=free, f_y=0, f_z=0, rotf_x=0, rotf_y=0, rotf_z=0*
B	*f_x=0, f_y=free, f_z=0, rotf_x=0, rotf_y=0, rotf_z=0*
C	*f_x=free, f_y=-3 mm, f_z=0, rotf_x=0, rotf_y=0, rotf_z=0*
D	*free*

The values of the Poisson's ratio (NPR) and Young's modulus were calculated using the following equations [5,6,9,12,17,18]:

$$\nu = -\frac{\varepsilon_x}{\varepsilon_y} = -\frac{\delta_x \cdot L_y}{\delta_y \cdot L_x} \tag{10}$$

$$E_y = \frac{\sigma_y}{\varepsilon_y} = \frac{F_y / A}{\delta_y / L_y} = \frac{F_y \cdot L_y}{\delta_y \cdot t \cdot L_x} \tag{11}$$

where $\varepsilon_x$and ε_y are the strains in the horizontal and vertical directions, respectively; u_x and u_y are the displacements in the horizontal and vertical directions; σ_y is the normal stress in the vertical direction; F_y is the reaction force in the vertical direction; and A is the cross-sectional area occupied by the structure in space.

3.1. Validation of numerical results

The numerical results obtained in this study were validated against theoretical results for the 2D-AS and *i*2D-AS structures, considering variations in the parameter ah [6,9]. In Ref. [6,9], the theoretical influence of Young's modulus and Poisson's ratio (NPR) was calculated for the 2D-AS structure, whereas Ref. [6] only compared the results for NPR. The obtained results are summarized in Table 7. Based on this validation, the numerical model was subsequently applied to the remaining two structures, *t*2D-AS and 2D-SS.

Table 7: Validation of numerical results for 2D-AS and *i*2D-AS against theoretical results from Refs. [6,9].

Model	*Parameter*	*Negative Poisson Ratio*			*Young's modulus [MPa]*		
	ah	*Current*	*Theory[6,9]*	*Error [%]*	*Current*	*Theory[6,9]*	*Error [%]*
2D-AS	*10*	-0.1267	-0.1205	5.15	0.3505	0.3605	2.77
	12	-0.2317	-0.2328	0.47	0.3813	0.3930	2.98
	14	-0.3339	-0.3387	1.42	0.4121	0.4263	3.33
	16	-0.4280	-0.4339	1.36	0.4415	0.4535	2.65
	18	-0.5089	-0.5145	1.09	0.4714	0.4833	2.46
*i*2D-AS	*10*	-0.1610	-0.1753	8.16	0.4002	0.4279	6.47
	12	-0.2524	-0.2635	4.21	0.3951	0.4225	6.49
	14	-0.3477	-0.3553	2.14	0.4018	0.4290	6.34
	16	-0.4411	-0.4451	0.9	0.4175	0.4448	6.12
	18	-0.5253	-0.5258	0.1	0.4391	0.4678	6.14

4. RESULTS OF THE NUMERICAL ANALYSIS

Under vertical loading, all four structures exhibit significant stress concentrations at the points where the vertical and horizontal beams connect with the arches (2D-AS, *i*2D-AS, and *t*2D-AS), or at the intersection of three beams, as observed in the 2D-SS structure. In the 2D-AS, *t*2D-AS, and 2D-SS structures, stress concentrations also occur at locations where other beams intersect at certain angles. This phenomenon is avoided in the *i*2D-AS structure, as these beams are replaced by a circular arch. Figure 6 presents the Von Mises stress nephograms for all four types of structures, with geometric parameters $ah = 14$ mm and $bh = 14$ mm.

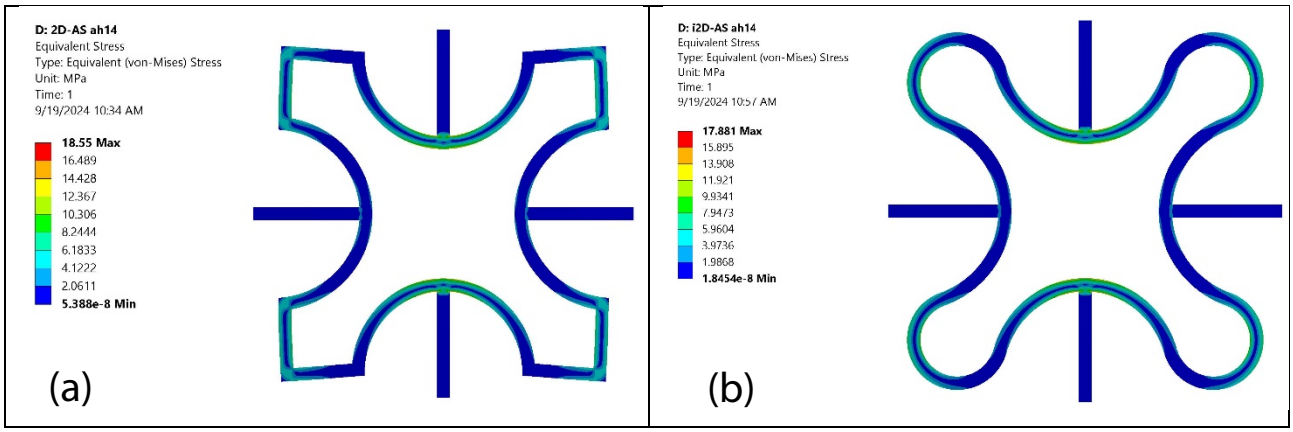

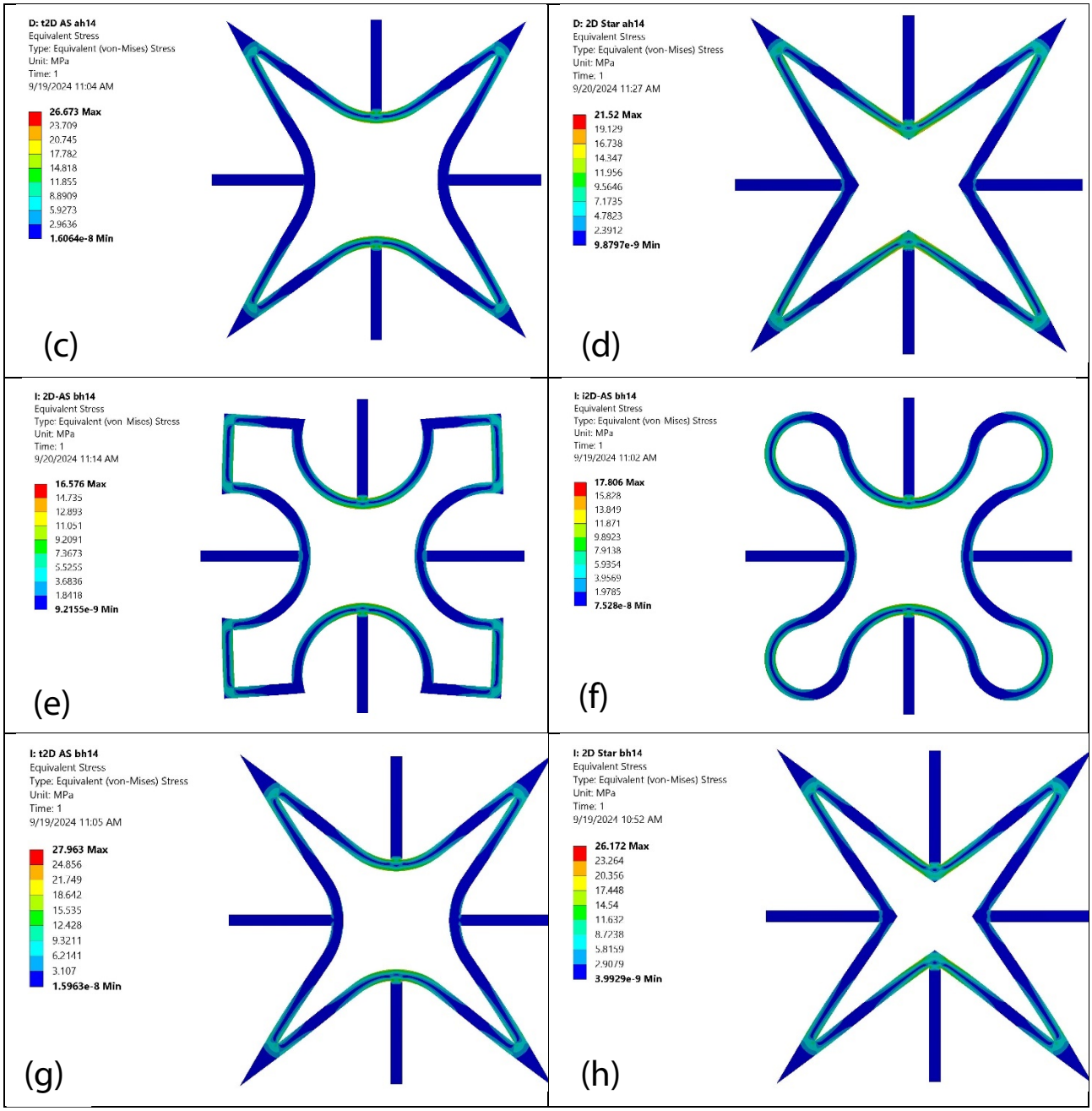

Figure 6: Von-Mises stress nephograms for: (a-d) *ah14* [5]and (e-h) *bh14*

The results for Poisson's ratio (NPR) and Young's modulus corresponding to the variation of the parameter $ah$are presented in Table 8, while Table 9 shows the results for the variation of the parameter bh. Additionally, the results are graphically illustrated in Fig. 7(a–d).

Table 8: Values of Poisson's ratio and Young's modulus for the variation of parameter ah.

ah		*10*	*12*	*14*	*16*	*18*
2D-AS	ν	-0.1267	-0.2317	-0.3339	-0.4280	-0.5089
	E_y *[MPa]*	0.3505	0.3813	0.4121	0.4415	0.4714
*i*2D-AS	ν	-0.1610	-0.2524	-0.3477	-0.4411	-0.5253
	E_y *[MPa]*	0.4002	0.3951	0.4018	0.4176	0.4391
*t*2D-AS	ν	-0.3733	-0.3861	-0.3992	-0.4104	-0.4152
	E_y *[MPa]*	0.6364	0.6490	0.6675	0.6936	0.7337
2D-SS	ν	-0.3987	-0.4249	-0.4587	-0.5022	-0.5589
	E_y *[MPa]*	0.6364	0.6437	0.6539	0.6686	0.6923

Table 9: Values of Poisson's ratio and Young's modulus for the variation of parameter bh.

bh		*10*	*12*	*14*	*16*
2D-AS	ν	-0.0566	-0.2175	-0.3758	-0.5204
	E_y *[MPa]*	0.4005	0.3917	0.3784	0.3598
*i*2D-AS	ν	-0.0808	-0.2352	-0.4021	-0.5709
	E_y *[MPa]*	0.3685	0.3900	0.4122	0.4341
*t*2D-AS	ν	-0.1507	-0.3427	-0.5207	-0.6495
	E_y *[MPa]*	0.5809	0.6358	0.7255	0.9792
2D-SS	ν	-0.1740	-0.3811	-0.5808	-0.7454
	E_y *[MPa]*	0.5842	0.6316	0.7033	0.9072

In Figures 7(a–b), the *t*2D-AS structure exhibits the lowest values of Poisson's ratio (NPR). On the other hand, as shown in Figures 7(c–d), the other three structures display lower values of Young's modulus. The *t*2D-AS structure, which has the lowest relative density compared to the others, also shows a lower Young's modulus than the 2D-SS structure. The 2D-AS and i2D-AS structures exhibit even lower Young's modulus values under certain conditions.

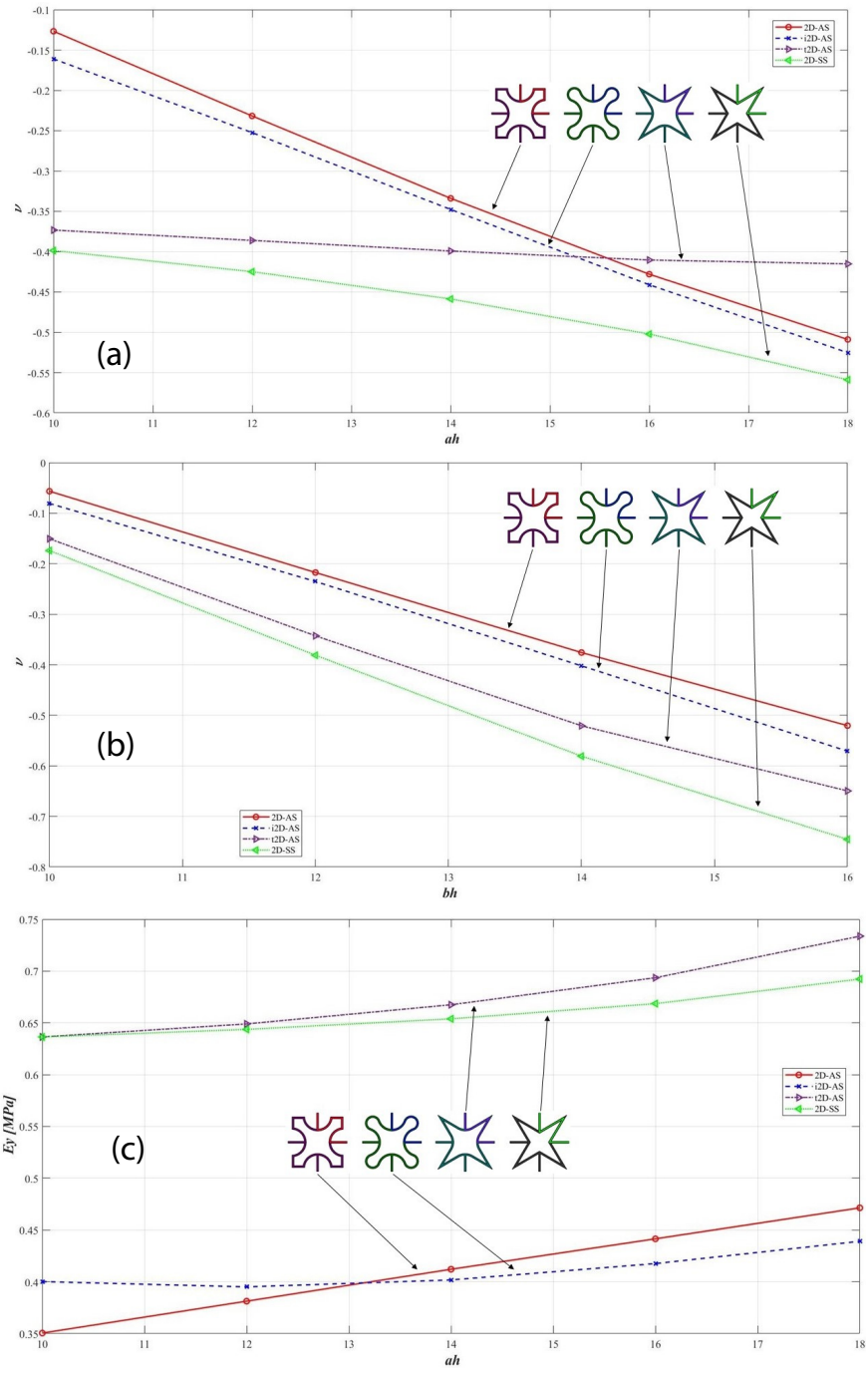

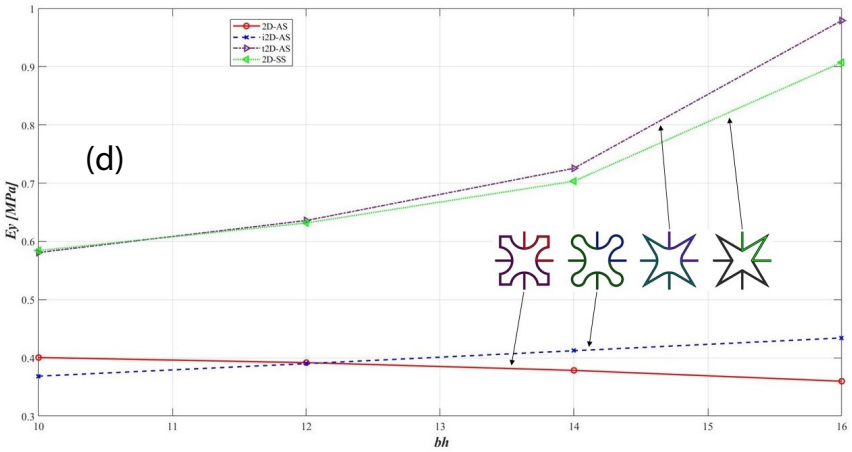

Figure 7: Variation of Poisson's ratio (NPR) and Young's modulus with geometric parameters: (a) ah [5]; (b) bh.

For the ah parameter range of 10–12 mm, the 2D-AS structure demonstrates the highest Young's modulus values, whereas for larger ah values, the i2D-AS structure exhibits the highest Young's modulus (Figure 7(c)). With variation in the bhparameter (Figure 7(d)), in the range of 10–12 mm, i2D-AS shows the best Young's modulus values, while for higher bh values, 2D-AS achieves the highest Young's modulus results.

4.1. Verification of NPR on the $n \times n$ model

In this section, a numerical analysis of the NPR behavior of the $n \times n$ structural models are performed. In the previous analysis of a single PBC structure, an element size of 0.25 mm was employed. To avoid an excessive number of elements in the $n \times n$ simulations, the mesh element size was increased to 1 mm. The same mesh generation approach was applied to the $n \times n$ models as in the single PBC case, except for the increased element size.

As a test case, a geometric parameter value of $ah = 14$mm was selected for all structures. The periodic boundary conditions applied to the $n \times n$ model is illustrated in Fig. 8(a), while the generated mesh for the $n \times n$ model is shown in Fig. 8(b). The boundary conditions applied to the $n \times n$ model is identical to those used for a single unit cell (Table 6). The obtained results are summarized in Table 10.

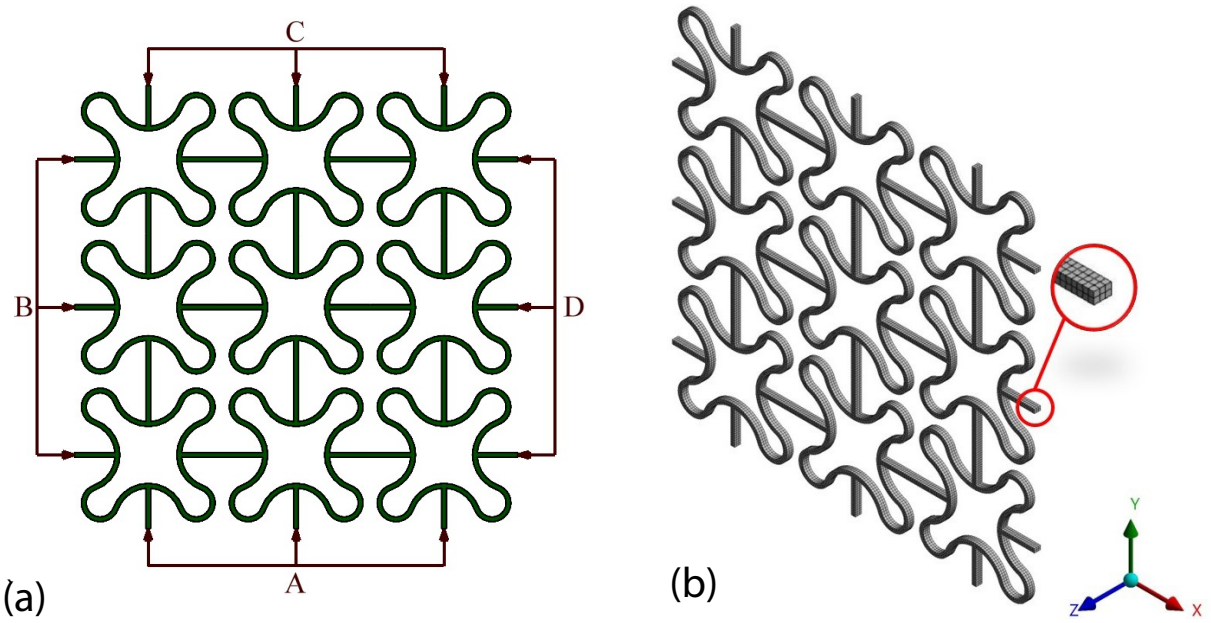

Figure 8: Example of the $n \times n$model for the *i*2D-AS structure:
(a) periodic boundary conditions (PBC); (b) generated mesh.

Table 10: Values of Poisson's ratio (NPR), "Skewness", and "Orthogonal Quality" for the $n \times n$model with $ah = 14$mm.

nxn model		*1x1*	*3x3*	*5x5*	*7x7*	*9x9*
2D-AS *ah14*	*ν*	-0.3327	-0.3325	-0.3333	-0.3330	-0.3335
	Skewness	0.3818	0.3776	0.3642	0.3730	0.3647
	Orthogonal	0.7024	0.7108	0.7280	0.7189	0.7273

*i*2D-AS *ah14*	ν	-0.3469	-0.3471	-0.3468	-0.3470	-0.3469
	Skewness	0.3842	0.4129	0.4134	0.4078	0.4007
	Orthogonal	0.7010	0.6952	0.6895	0.6952	0.7010
*t*2D-AS *ah14*	ν	-0.3937	-0.3949	-0.3950	-0.3890	-0.3894
	Skewness	0.2759	0.4087	0.4265	0.6768	0.6751
	Orthogonal	0.8060	0.6940	0.6763	0.3257	0.3281
2D-SS *ah14*	ν	-0.4521	-0.4535	-0.4537	-0.4509	-0.4510
	Skewness	0.3545	0.4239	0.4454	0.6790	0.6779
	Orthogonal	0.7073	0.6743	0.6529	0.3290	0.3299

As shown in Table 10, the mesh quality of the $n \times n$ models are satisfactory when evaluated against the criteria listed in Table 4. Figures 9(a–d) graphically illustrate the deviation of the $n \times n$ models with an element size of 1 mm in comparison with the single PBC structures modeled using an element size of 0.25 mm.

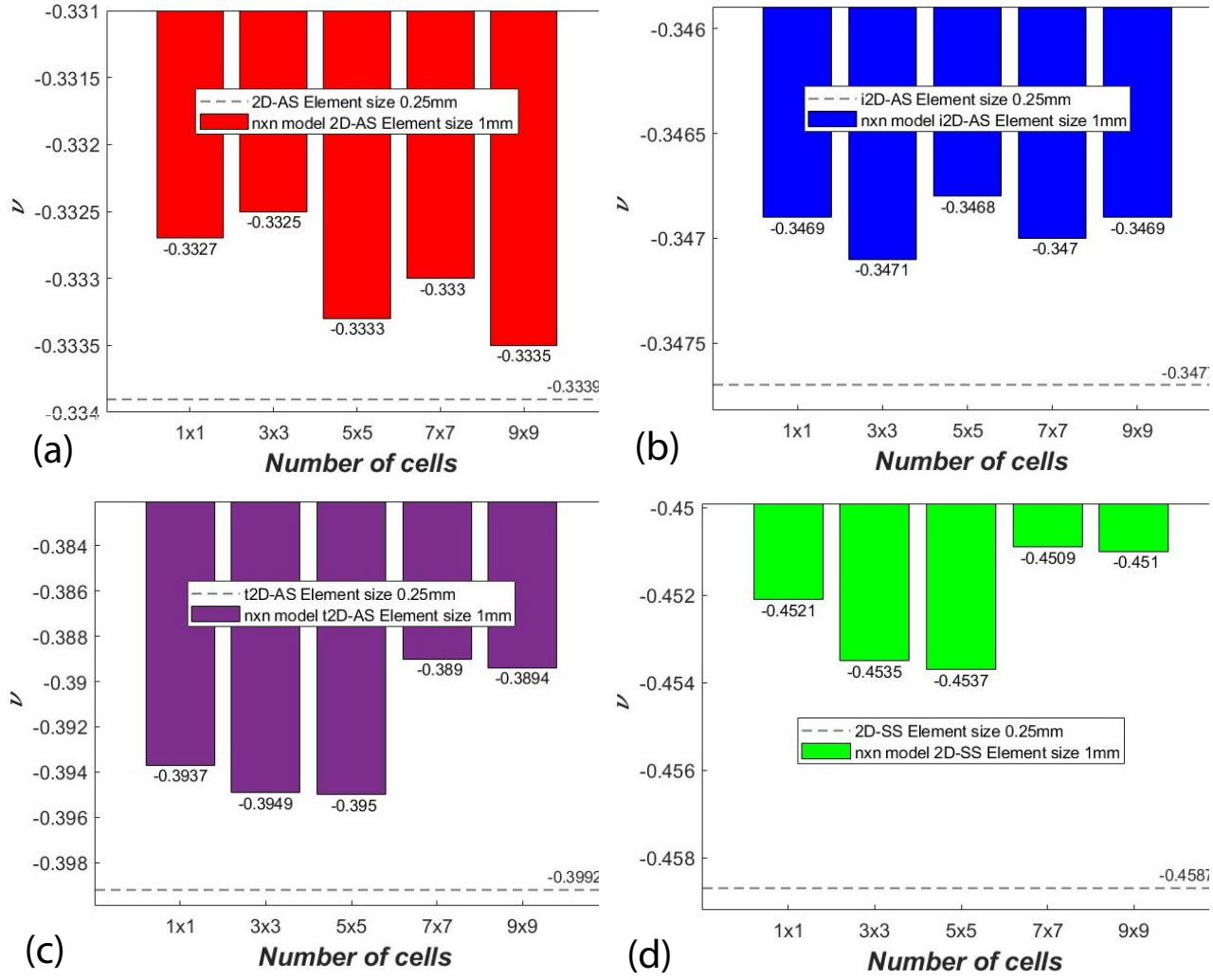

Figure 9: Deviation of Poisson's ratio (NPR) for the $n \times n$ model with an element size of 1 mm compared to the single PBC model with an element size of 0.25 mm: (a) 2D-AS, $ah = 14$mm; (b) i2D-AS, $ah = 14$mm; (c) t2D-AS, $ah = 14$mm; and (d) 2D-SS, $ah = 14$mm.

5. CONCLUSION

The objective of this study was to numerically determine and compare the mechanical properties of four different star-shaped structures. By modifying the geometry of the conventional 2D-AS structure, a new topology, denoted as t2D-AS, was introduced. The results showed that the *t*2D-AS structure is the lightest among the four considered configurations. Despite its reduced mass, the obtained values of the negative Poisson's ratio (NPR) and Young's modulus for the t2D-AS structure are only slightly lower than those of the traditional 2D-SS structure for the selected geometric parameters, indicating a favorable stiffness-to-weight ratio.

Furthermore, the *i*2D-AS structure, due to the presence of arches, exhibited the highest Young's modulus for most variations of the geometric parameters a_h and b_h, demonstrating its superior stiffness characteristics. The numerical analysis also revealed that the use of a coarser finite element mesh leads to NPR values that are in good agreement with those obtained using a finer mesh, confirming the reliability of the numerical approach.

Future research should focus on the development of analytical and further numerical models for the newly proposed t2D-AS structure. In addition, a comprehensive investigation of the energy absorption capabilities of all four structures would be of significant interest and practical relevance.

ACKNOWLEDGEMENTS

This paper is a result of the research conducted within the project grant number 451-03-137/2025-03/200108 supported by the Ministry of Science, Technology and Innovation of the Republic of Serbia and the CEEPUS project grant "Building Knowledge and Experience Exchange in CFD - RS-1012-10-2425" supported by the Central European Exchange Program for University Studies.

REFERENCES

[1] T.-C. Lim, "Mechanics of metamaterials with negative parameters", Springer, Singapore (Singapore), https://doi.org/10.1007/978-981-15-6446-8, (2020)

[2] T.-C. Lim, "Auxetic materials and structures", Springer, Singapore (Singapore), https://doi.org/10.1007/978-981-287-275-3, (2015)

[3] J. P. Ren, Z. P. Gu, A. G. Zhao, C. G. Huang, and X. Q. Wu, "Enhancing energy absorption of star-shaped honeycombs by utilizing negative Poisson's ratio effect under high-velocity impact", International Journal of Impact Engineering, Vol. 202, p. 105297. https://doi.org/10.1016/j.ijimpeng.2025.105297, (2025)

[4] K. K. Saxena, R. Das, E. P. Calius, "Three decades of auxetics research – materials with negative Poisson's ratio: A review", Advanced Engineering Materials, Vol. 18(11), pp. 1847–1870, https://doi.org/10.1002/adem.201600053, (2016)

[5] V. Sinđelić, S. Ćirić-Kostić, A. Nikolić, and N. Bogojević, "Numerical analysis of four types of arc star shaped auxetic structures", Proceedings of the11th International Scientific Conference Research and Development of Mechanical Elements and Systems IRMES (2025), Niš (Serbia), pp. 95–99, https://doi.org/10.46793/IRMES25.095S, (2025)

[6] V. Sinđelić, A. Nikolić, G. Minak, N. Bogojević, and S. Ćirić Kostić, "An improved 2D arc-star-shaped structure with negative Poisson's ratio: In-plane analysis", Materials Today Communications, Vol. 37, p. 107593. https://doi.org/10.1016/j.mtcomm.2023.107593, (2023)

[7] L. Ai and X.-L. Gao, "An analytical model for star-shaped re-entrant lattice structures with the orthotropic symmetry and negative Poisson's ratios", International Journal of Mechanical Sciences, Vol. 145, pp. 158–170, https://doi.org/10.1016/j.ijmecsci.2018.06.027, (2018)

[8] Z. Zheng, D. Chen, C. Xie, L. Li, and C. Lin, "In-plane analysis of an adjustable structure with negative Poisson's ratio and superior lightweight design", Smart Materials and Structures, Vol. 34(7), p. 075005. https://doi.org/10.1088/1361-665X/ade8bf, (2025)

[9] Z.-Y. Zhang, J. Li, H.-T. Liu, and Y.-B. Wang, "Novel 2D arc-star-shaped structure with tunable Poisson's ratio and its 3D configurations", Materials Today Communications, Vol. 30, p. 103016. https://doi.org/10.1016/j.mtcomm.2021.103016, (2022)

[10] Anonymous, ANSYS Mechanical APDL Element Reference, Canonsburg, PA 15317, 2011.

[11] Anonymous, Introduction to ANSYS Meshing, 2012.

[12] V. Sinđelić, S. Ćirić-Kostić, A. Nikolić, N. Bogojević, and G. Minak, "Analytical and numerical approach for determining the mechanical properties of a novel 3D double arc star-shaped structure with two different cross-sections", Mechanics of Solids, Vol. 60, pp. 3993–4016, https://doi.org/10.1134/S0025654425601958, (2025)

[13] T. Wang, Z. Li, L. Wang, X. Zhang, and Z. Ma, "In-plane elasticity of a novel arcwall-based double-arrowed auxetic honeycomb design: Energy-based theoretical analysis and simulation", Aerospace Science and Technology, Vol. 127, p. 107715, https://doi.org/10.1016/j.ast.2022.107715, (2022)

[14] Q. Zhang, Y. Zhu, Y. Wang, and J. Li, "A novel barbell-shaped perforated auxetic metastructure with superior auxetic effect", Physica Status Solidi (b), Vol. 260(12), p. 2300351, https://doi.org/10.1002/pssb.202300351, (2023)

[15] X. Zhang, C. Lu, R. Li, and T. Xie, "Study of rhombic star-shaped honeycomb with tunable Poisson's ratio and elastic modulus properties", Applied Physics A, Vol. 130, No. 91, https://doi.org/10.1007/s00339-023-07256-y, (2024)

[16] H.S. Kavakli and D. Ali, "Enhancing the mechanical properties of auxetic metamaterials by incorporating non-rectangular cross sections into their component rods: A finite element analysis", Physica Status Solidi (b), Vol. 260(3), p. 2200194, https://doi.org/10.1002/pssb.202200194, (2023)

[17] V. Sinđelić, S. Ćirić-Kostić, N. Bogojević, and A. Nikolić, "Numerical analysis of the modified 3D Arc-star-shaped auxetic structure", Proceedings of KOD 2024, Balatonfüred (Hungary), pp. 695–705, https://doi.org/10.1007/978-3-031-80512-7_68, (2025)

[18] V. Sinđelić, A. Nikolić, N. Bogojević, S. Ćirić-Kostić, and G. Minak, "Analytical and numerical analysis of the modified 2D arc-star-shaped structure with negative Poisson's ratio", Engineering Today, Vol. 3, pp. 55–62. https://doi.org/10.5937/engtoday2400004S, (2024)